chemistry

MDPI

Article

Self-Heating Performance of Magnetite Doped with Cobalt/Zinc Nanoparticles: Impact of Magnetic Field, Coating Agent, and Dispersing Solvent

Enaam A. Al-Harthi [1,*], Ghaida H. Munshi [1], Jamilah M. Al-Ahmari [1] and Mohamed S. A. Darwish [2,*]

[1] Department of Chemistry, College of Science, University of Jeddah, Jeddah 21959, Saudi Arabia; gmunshi@uj.edu.sa (G.H.M.); gmalahmary@uj.edu.sa (J.M.A.-A.)
[2] Egyptian Petroleum Research Institute, 1 Ahmed El-Zomor Street, El Zohour Region, Nasr City, Cairo 11727, Egypt
* Correspondence: ealharthy@uj.edu.sa (E.A.A.-H.); msa.darwish@gmail.com (M.S.A.D.)

Abstract

Fabrication of magnetic materials via a facile and environmentally favorable process with high self-heating performance is quite favored for biomedical applications. To tackle this challenge, magnetic ferrite nanoparticles were developed through an ultrasonic-assisted coprecipitation process. Magnetite (Fe_3O_4), magnetite doped with cobalt nanoparticles ($Co_{0.4}Fe_{2.6}O_4$), and magnetite doped with cobalt/zinc nanoparticles ($Zn_{0.15}Co_{0.25}Fe_{2.6}O_4$) were synthesized using ultrasonic-assisted coprecipitation techniques. Specific loss power (SLP) was estimated to optimize the heating influence under varied magnetic fields, coating agents, and dispersing solvents. Magnetite doped with cobalt/zinc nanoparticles demonstrated elevated SLP 110 W/g with preferable hyperthermic performance, where AMF conditions did not surpass the safety border for human exposure. The self-heating performance of magnetite doped with cobalt/zinc nanoparticles increased with increasing strength at a constant frequency. The self-heating performance of magnetite nanoparticles increased with increasing frequency at constant strength. Hence, the prepared magnetite doped with cobalt/zinc nanoparticles by the ultrasonic-assisted coprecipitation process can be appropriate for biomedical applications.

Keywords: self-heating; magnetic ferrite nanoparticle; hyperthermia; biomedical applications

1. Introduction

Ferrite nanoparticles (FNs) have been widely used in environmental, industrial, and biomedical fields [1–6]. FNs have special behaviors, like high magneto-crystalline anisotropy and coercivity [7,8]. The composition, size, morphology, and magnetic behavior were controlled by the conditions and selected fabrication process [9–11]. However, due to factors that affect the fabrication techniques, a slight change in any parameter may result in the obtained ferrite nanoparticles with special behaviors [1]. Thus, the influences of medium, temperature, reaction pH, and time are investigated when fabricating materials for certain fields [12,13]. However, FN agglomeration fosters magnetic behaviors as the loss of size-dependent attitude in the particles [14]. Their self-heating efficiency is often deficient, which is believed to be the essential challenge to the evolution of practical cancer therapy [15–17]. Currently, two types of magnetic particles are utilized in clinical tests, modified with polysaccharides and silica. Ferumoxytol was primarily tested as a contrast agent for MRI [18]. NanoTherm® nanoparticles were approved for the hyperthermia

Check for updates

Academic Editor: Gurumurthy Hegde

Received: 29 December 2025
Revised: 11 February 2026
Accepted: 13 February 2026
Published: 16 February 2026

Copyright: © 2026 by the authors. Licensee MDPI, Basel, Switzerland. This article is an open access article distributed under the terms and conditions of the Creative Commons Attribution (CC BY) license.

technique. Magnetite has an intrinsic magnetic ability that operates with an alternating magnetic field (AMF) and releases energy by relaxation processes [2]. FNs that can raise the temperature of the selected area >45 °C are fit for therapy [15]. A decrease in therapy time is demanded for safe treatment. Size and chemical composition of magnetic nanostructures plays a role in magnetization; control is important for the efficiency of treatment. Heating performance is impacted by magnetic properties, field conditions, and nanoparticle size. Specific loss power (SLP) is applied to estimate the energy amount per nanoparticle under AMF [16–29]. It was detected that the particle size from 20 to 70 nm showed good thermal efficiency [24]. Recorded values for SLP in the reports are 10–100 Wg^{-1} [26]. SLP is not a fair hyperthermia parameter in comparison with other works because the input magnetic energy is not pointed out and normalized. For the magnetic nanoparticle with bad hyperthermia performance, it still showed good SLP if the input high magnetic power is quite large. The Intrinsic Loss Parameter (ILP) is the magnetic heating capability of a particle, normalizing the SLP to H^2 and f. This normalization creates a material-specific parameter that is independent of the experimental conditions, allowing for accurate comparison of heating properties across different tests and particles. ILP is a critical metric for estimating MNP performance in magnetic hyperthermia treatments for conditions like cancer. Thus, great efforts have been made to fabricate particles with high ILP. MNPs have numerous advantages; they are biocompatible, thermal, colloidal, and chemically stable. However, characteristics of synthesized MNPs depend on the synthesis technique used. That is why we must choose the most convenient method for the application according to the properties needed. The main challenge in the fabrication of magnetic materials is how to enhance the monodisperse behavior of particles with high SLP by using simple and environmentally friendly techniques. The stoichiometric equation for the preparation of magnetite via the generally used chemical coprecipitation technique includes iron (II) and iron (III) salts in a (1:2) molar ratio under alkaline conditions.

$$Fe^{2+} + 2Fe^{3+} + 8OH^- \rightarrow Fe_3O_4 + 4H_2O$$

In spinel materials, variations in Fe^{2+}/Fe^{3+} ratios often accompany the formation of cation vacancies or changes in the crystal lattice, which affect the overall structure. Using a non-stoichiometric ratio enables us to gain insight into their chemical and physical behavior. Tuning the compositions is critical to improving the magnetic properties, which valuably assists in enhancing the hyperthermia performance of magnetic nanoparticles. The current work aimed to fabricate magnetic ferrite nanoparticles using ultrasonic-assisted coprecipitation. This technique remarkably affects nanoparticle fabrication by producing small, uniform particles with high surface area for leading dispersion compared to conventional techniques. This is carried out through the cavitation impact of an ultrasound, which produces localized high temperature and pressure that support nucleation and decrease particle growth. The particles were fabricated with environmentally friendly techniques without organic solvents and an effortless process with inexpensive components. The fabricated particles show superior self-heating efficiency by producing energy with AMF. In this work, self-heating performances of magnetite (Fe_3O_4), magnetite doped with cobalt nanoparticles ($Co_{0.4}Fe_{2.6}O_4$), and magnetite doped with cobalt/zinc nanoparticles ($Zn_{0.15}Co_{0.25}Fe_{2.6}O_4$) were fabricated by ultrasonic-assisted coprecipitation techniques. The thermal and self-heating behaviors of the nanoparticles were determined based on SLP. SLP was estimated to optimize the heating impacts under varied magnetic field conditions.

2. Materials and Methods

2.1. Materials

$FeCl_3 \cdot 6H_2O$ (≥99%), $FeCl_2 \cdot 4H_2O$ (≥99%), $CoCl_2 \cdot 6H_2O$ (≥98%), $ZnCl_2$ (≥98%), and ammonium hydroxide (concentration 16.4 mol/L) were ordered (Sigma Aldrich, St. Louis, MO, USA).

2.2. Magnetite Nanoparticles (Fe_3O_4) Fabrication

$FeCl_3 \cdot 6H_2O$ (0.59 mole) and $FeCl_2 \cdot 4H_2O$ (0.399 mole) were mixed in distilled water (DW) (50 mL) at 60 °C until complete homogenous solution was obtained. Ammonium hydroxide (20 mL) was added dropwise and stirred in a sonicated bath (YNLH0306-20, Yunyisonic, Shenzhen, China, frequency: 20 kHz automatic tracking, ultrasonic power: 2200 W, temperature: 25 °C) for 30 min. The precipitate of magnetite nanoparticles was washed with DW and then dried (sample S1).

2.3. Magnetite Doped with Cobalt Nanoparticles ($Co_{0.4}Fe_{2.6}O_4$) Fabrication

$FeCl_3 \cdot 6H_2O$ (0.59 mole), $FeCl_2 \cdot 4H_2O$ (0.399 mole), and $CoCl_2 \cdot 6H_2O$ (0.199 mole) were mixed in DW (50 mL) at 60 °C until a complete homogenous solution was obtained. Ammonium hydroxide (20 mL) was added dropwise and stirred in a sonicated bath (frequency: 20 kHz automatic tracking, ultrasonic power: 2200 W, temperature: 25 °C) for 30 min. The precipitate of nanoparticles was washed with DW and then dried (sample S2).

2.4. Magnetite Doped with Cobalt/Zinc Nanoparticles ($Zn_{0.15}Co_{0.25}Fe_{2.6}O_4$) Fabrication

$FeCl_3 \cdot 6H_2O$ (0.59 mole), $FeCl_2 \cdot 4H_2O$ (0.399 mole), $CoCl_2 \cdot 6H_2O$ (0.199 mole), and $ZnCl_2$ (0.199 mole) were mixed in DW (50 mL) at 60 °C until a complete homogenous solution was obtained. Ammonium hydroxide (20 mL) was added dropwise and stirred in a sonicated bath (frequency: 20 kHz automatic tracking, ultrasonic power: 2200 W, temperature: 25 °C) for 30 min. The precipitate was washed with DW and then dried (sample S3). For coating with sodium citrate, particles (0.1 g) were added to a solution of (0.5 g sodium citrate (≥99%, Sigma Aldrich, MO, USA), in 25 mL DW) and mixed via an ultrasonic bath for 4 h.

2.5. Hyperthermia Performance

Nanoparticle sample (50 mg) was dissolved in distilled water (6 mL). Heating performance, affecting a quasi-adiabatic regime in the first ten seconds, was measured. The temperature was measured using an Osensa optic temperature, PRB-100, OSENSA Innovations, Burnaby, BC, Canada, measurement cable. SLP values were investigated to optimize the heating performance by using varied field conditions of frequency (f) and magnetic field (H).

$$SLP = [Cp/m] \times [dT/dt]$$

where dT/dt (time/dependent temp.), Cp (4.184) and m (mass).

2.6. In Vitro Cytocompatibility Test

The toxicity of the fabricated samples was investigated using culturing NIH-3T3 cells (Dojindo Laboratories, Kumamoto, Japan) by a WST assay. The seeding density of 5×10^4 cells/well in a 24-well plate was measured, and cell were incubated for one day in DMEM (Dulbecco's Modified Eagle Medium, Hyclone, Logan, UT, USA) supplemented with 10% FBS (Fetal Bovine Serum, Hyclone, UT, USA) and 1% antibiotics. Then, the culture medium (1 mL) containing the nanoparticles was added to the cells and incubated for an additional day. The sample solution was removed and washed with DPBS. Then, fresh culture medium (0.5 mL) and WST assay solution (0.05 mL, Dojindo Laboratories,

Kumamoto, Japan) were added and incubated for two hours. An amount of 0.1 mL of the solution from the well was moved to a new plate, and the absorbance at 450 nm was investigated using a microplate reader. A_c and A_s are absorbances of control and solution samples, respectively. The cell viability was normalized to the control using the following formula:

$$\text{Cell Viability (\%)} = (A_c - A_s)/A_c \times 100$$

2.7. Characterizations

Hydrodynamic diameter is provided by dynamic light scattering (DLS). DLS and Zeta potential measurements were recorded using a Zeta-potential and Particle Size Analyzer (ELSZ-2000; Photal Otsuka Electronics, Osaka, Japan). For DLS and Zeta potential tests, a suspension of 50 mg nanoparticles in 6 mL deionized water to obtain a ferrofluid at a concentration of 8.3 mg mL^{-1} was subjected to ultrasound (5 min) before the analyses; the corresponding pH values for Zeta potential measurements were 3.8, 4, 4.3, and 4.1 for S1, S2, uncoated S3, and coated S3, respectively. The metal contents were measured by inductively coupled plasma-optical emission spectroscopy (ICP-OES; Optima 8300, PerkinElmer, Waltham, MA, USA). An amount of 0.1 g of the nanoparticles dispersed in 25 mL D.I. water (Deionized Water) was subjected to ultrasound before the analyses. The quantitation range for cost elements was 50 ppm for ICP-OES. The sample was made using an aqueous nitric acid solution. Additional dilution was performed to make the sample concentration according to the specified range. Nanoparticles phases were detected with XRD (X-ray Diffraction, Rigaku, Tokyo, Japan). The Scherrer equation was utilized to detect the crystallite size (grain):

$$Dp = \frac{K\lambda}{\beta cos\theta} \quad (1)$$

where grain sizes (Dp), β (FWHM), λ (1.5406), K (constant), θ (angle).

Magnetic behavior was detected using VSM Lake Shore 7400 series; Lake Shore Cryotronics, Westerville, OH, USA). UV-spectrophotometer (V-570, JASCO, Tokyo, Japan). Morphologies were detected with TEM (Transmission Electron Microscopy, Tecnai G2S Twin; Philips, Hillsboro, OR, USA).

3. Results

3.1. Particles Characterization

Tuning the compositions and sizes is critical to improving magnetization, which valuably assists in enhancing hyperthermia performance of nanoparticles. Magnetite nanoparticles (sample S1), magnetite doped with cobalt nanoparticles (sample S2), and magnetite doped with cobalt/zinc nanoparticles (sample S3) were fabricated using ultrasonic-assisted coprecipitation without organic solvents and with inexpensive components. The size and the morphology were studied using TEM (Figure 1). The size of the fabricated samples S1, S2, and S3 were 12.3 $\pm$ 3.2, 8 $\pm$ 2, and 25 $\pm$ 5 nm, respectively. DLS was used to investigate the mean hydrodynamic size. The sizes were 237, 302, and 575 nm for S1, S2, and S3, respectively (which was higher than that obtained using TEM analysis).

Surface charge was detected with Zeta potential values, which is an indicator of colloidal stability. The Zeta potentials of the fabricated samples S1, S2, and S3 were -39.32, 29.38, and 15.65 mV, respectively.

XRD was utilized to detect the crystallite size (grain) by the Scherrer equation and to identify the type of magnetic phase by matching the detected diffraction peaks with known patterns for specific nanoparticles (Figure 2). The peaks correspond to ICSD (98-015-8742) and were detected for the dominant magnetite nanoparticles phase (Fe_3O_4). The ferrite crystalline behaviors of magnetite doped with cobalt nanoparticles and magnetite doped

with cobalt/zinc nanoparticles were detected with JCPDS (221086). The estimated sizes for the fabricated samples S1, S2, and S3 were 11.7, 8, and 14.5 nm, respectively.

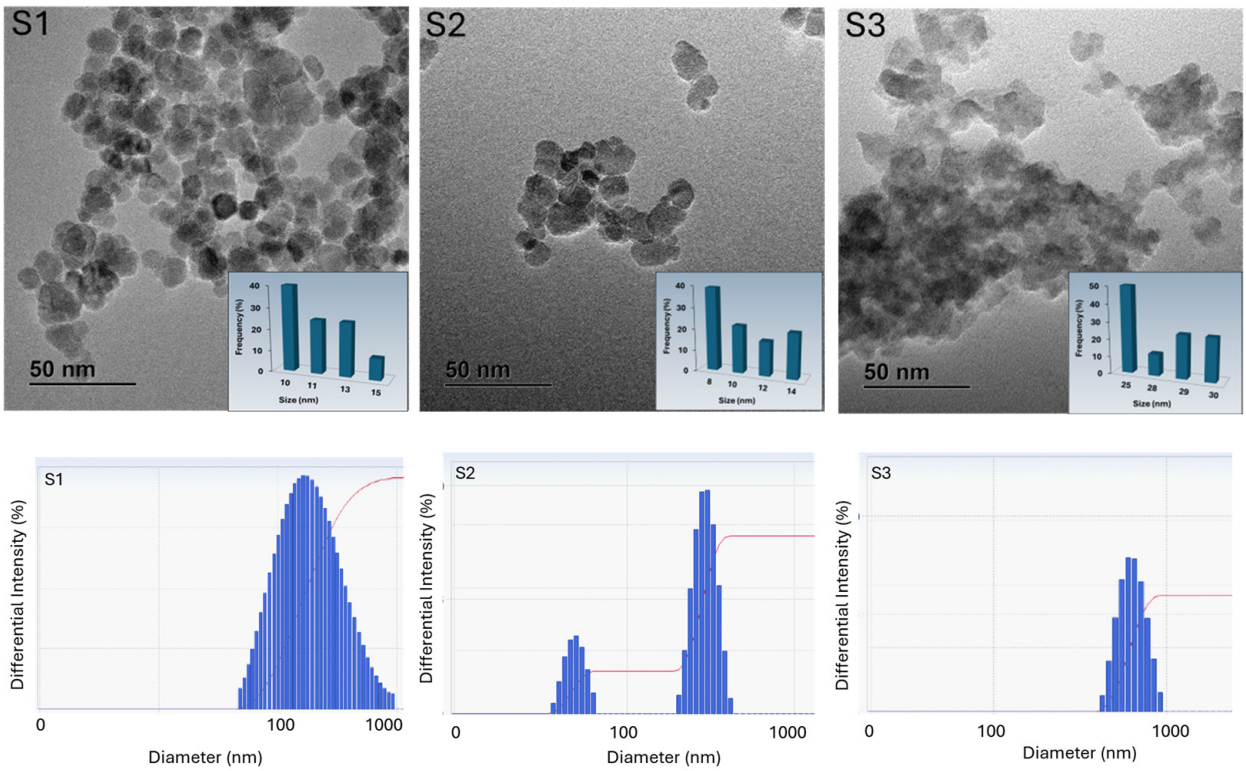


Figure 1. TEM and DLS of the fabricated samples S1, S2, and S3.

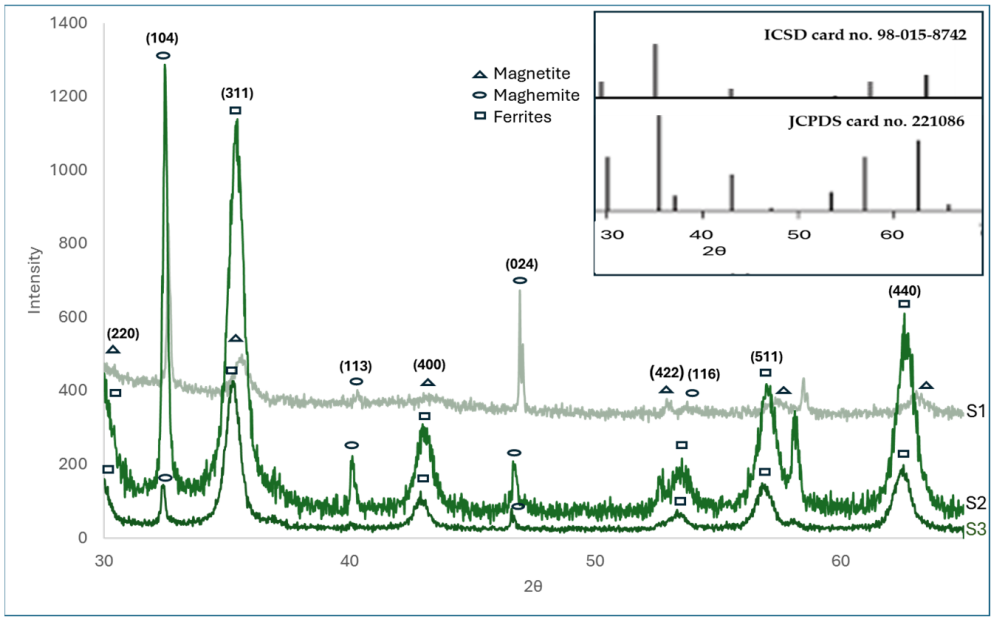


Figure 2. XRD of the fabricated samples S1, S2, and S3.

UV–Vis spectroscopy was used to detect the optical properties of the fabricated ferrites (Figure 3). The distinguishing peaks for ferrites were mainly located on the wavelength (nm) scale from 300 nm to 600 nm. The band gap energy for samples S1, S2, and S3 were 2.35, 2.50, and 2.4 eV. The lower level in the band gap could influence the photocatalytic character of the materials by minimizing the light needed for the reactions.

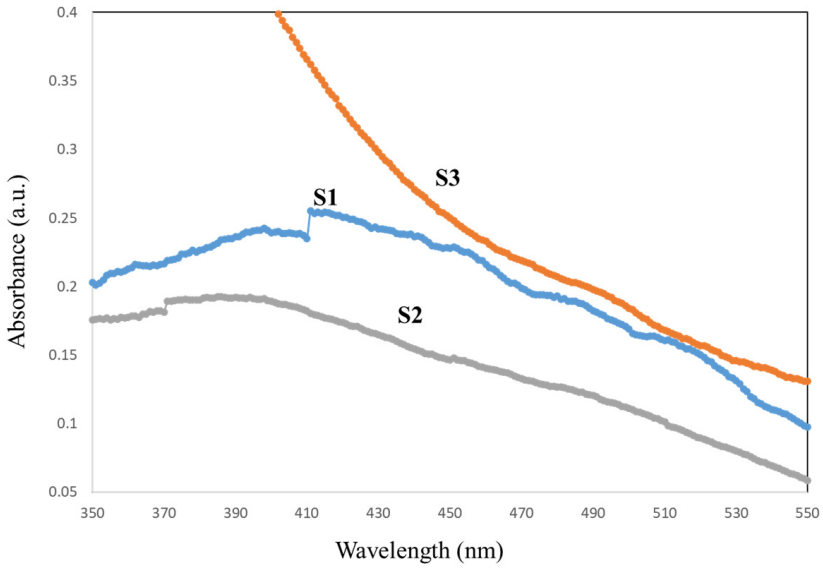


Figure 3. UV-Vis of the fabricated samples S1, S2, and S3.

The magnetic behavior for the fabricated magnetic particles was detected by VSM (Figure 4). Studying magnetic nanoparticles (MNPs) using VSM at room temperature is a standard method to determine their magnetic properties, particularly hysteresis loops which reveal parameters like saturation magnetization (Ms), remanence (Mr), and coercivity (Hc). It gives insights into the MNPs' potential applications, such as in magnetic hyperthermia by considering their restraint to the magnetic field and how they retain magnetization after the field is removed. Values of Hc, Mr, Ms, and squareness from the hysteresis loop were studied. The magnetization (M) and strength (H) curve confirmed the hysteresis loop and suggested the ferromagnetism of the fabricated particles. Magnetization saturation (Ms) values were 41.9, 50.7, and 50.6 emu/g for S1, S2, and S3 (Figure 4). The coercivity (Hc) values were 43, 190, and 247 Oe for S1, S2, and S3, respectively. The remanence values (Mr) were 3.8, 10.75, and 10.71 emu/g for samples S1, S2, and S3. Reduced remanence (SQ) [Mr/Ms]: The reduced remanence (SQ) values were 0.09, 0.212, and 0.211 emu/g for S1, S2, and S3.

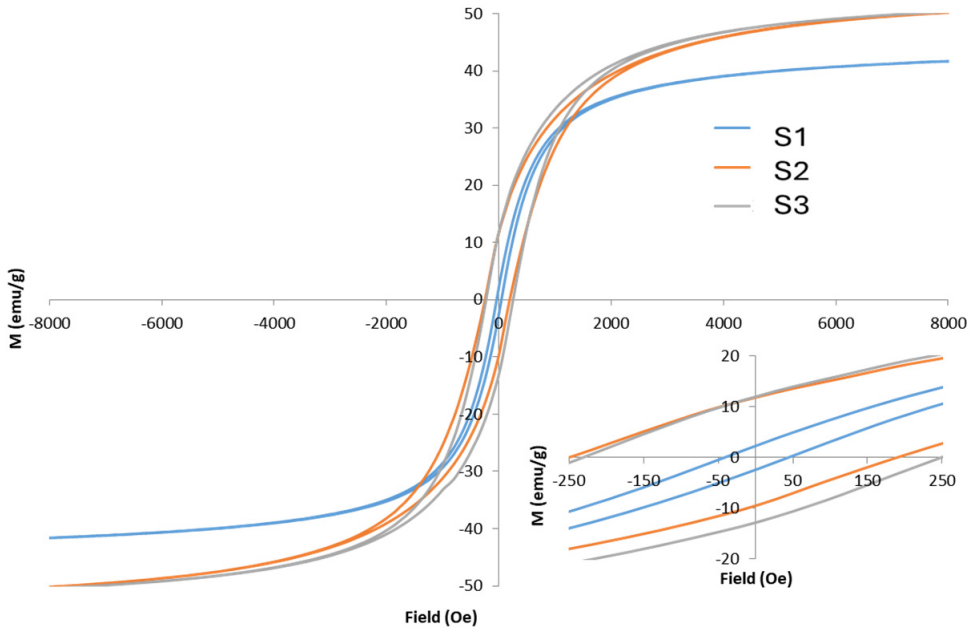


Figure 4. Magnetic properties of the fabricated samples S1, S2, and S3.

3.2. Hyperthermia Performance

Ferrite nanoparticles were able to produce thermal energy under alternative magnetic field (AMF) (Figure 5). For high-performance hyperthermia impact, magnetic nanoparticles should be a small size with a high magnetic saturation value. Increasing temperature is the basis for cancer treatment via induction heating techniques. The thermal time desired to gain 45 °C is influenced by several conditions such as magnetic field, medium, and concentration and particle size. The heating performances of the fabricated samples are listed In Table 1.

Table 1. The heating performances of the fabricated samples.

Sample	The Heating Performance (°C)	Magnetic Field Condition	The Safety Limit
S1	2.5	f = 106.6 kHz, H = 20 kA/m	Under the safety limit
	1.8	f = 159.8 kHz, H = 13.5 kA/m	
	4.3	f = 269.9 kHz, H = 13.5 kA/m	
	6.3	f = 381.6 kHz, H = 12.7 kA/m	
	7.6	f = 614.4 kHz, H = 9.5 kA/m	Over the safety limit
	7.3	f = 97 kHz, H = 40 kA/m	Under the safety limit
	8.6	f = 97 kHz, H = 50 kA/m	
S2	0.66	f = 106.6 kHz, H = 20 kA/m	Under the safety limit
	0.27	f = 159.8 kHz, H = 13.5 kA/m	
	0.4	f = 269.9 kHz, H = 13.5 kA/m	
	0.6	f = 381.6 kHz, H = 12.7 kA/m	
	0.2	f = 614.4 kHz, H = 9.5 kA/m	Over the safety limit
	16.18	f = 97 kHz, H = 40 kA/m	Under the safety limit
	32.3	f = 97 kHz, H = 50 kA/m	
S3	1.6	f = 106.6 kHz, H = 20 kA/m	Under the safety limit
	1.6	f = 159.8 kHz, H = 13.5 kA/m	
	3.8	f = 269.9 kHz, H = 13.5 kA/m	
	3.4	f = 381.6 kHz, H = 12.7 kA/m	
	0.8	f = 614.4 kHz, H = 9.5 kA/m	Over the safety limit
	30.2	f = 97 kHz, H = 40 kA/m	Under the safety limit
	47.2	f = 97 kHz, H = 50 kA/m	

The heating performances were evaluated at constant H = 13.5 kA/m, while changing f (159.8–269.9 kHz) (Figure 5b,c). The heating performance of sample S1 improved with the change f from 159.8 to 269.9 kHz. The temperature increased to 1.7 °C and 4.1 °C after 170 s under AMF applications at 159.8 and 269.9 kHz. As a result, the thermal performance of sample S1 elevated as the f increased under a constant H.

The heating performances were evaluated at a constant f = 97 kHz, while changing f 40–50 kA/m (Figure 5f,g). The heating performance improved as the strength increased. In sample S3, the temperature increased to 24.4 °C and 45 °C after 190 s of 40 and 50 kA/m. As a result, the thermal performance of sample S3 elevated as the H increased under a constant f.

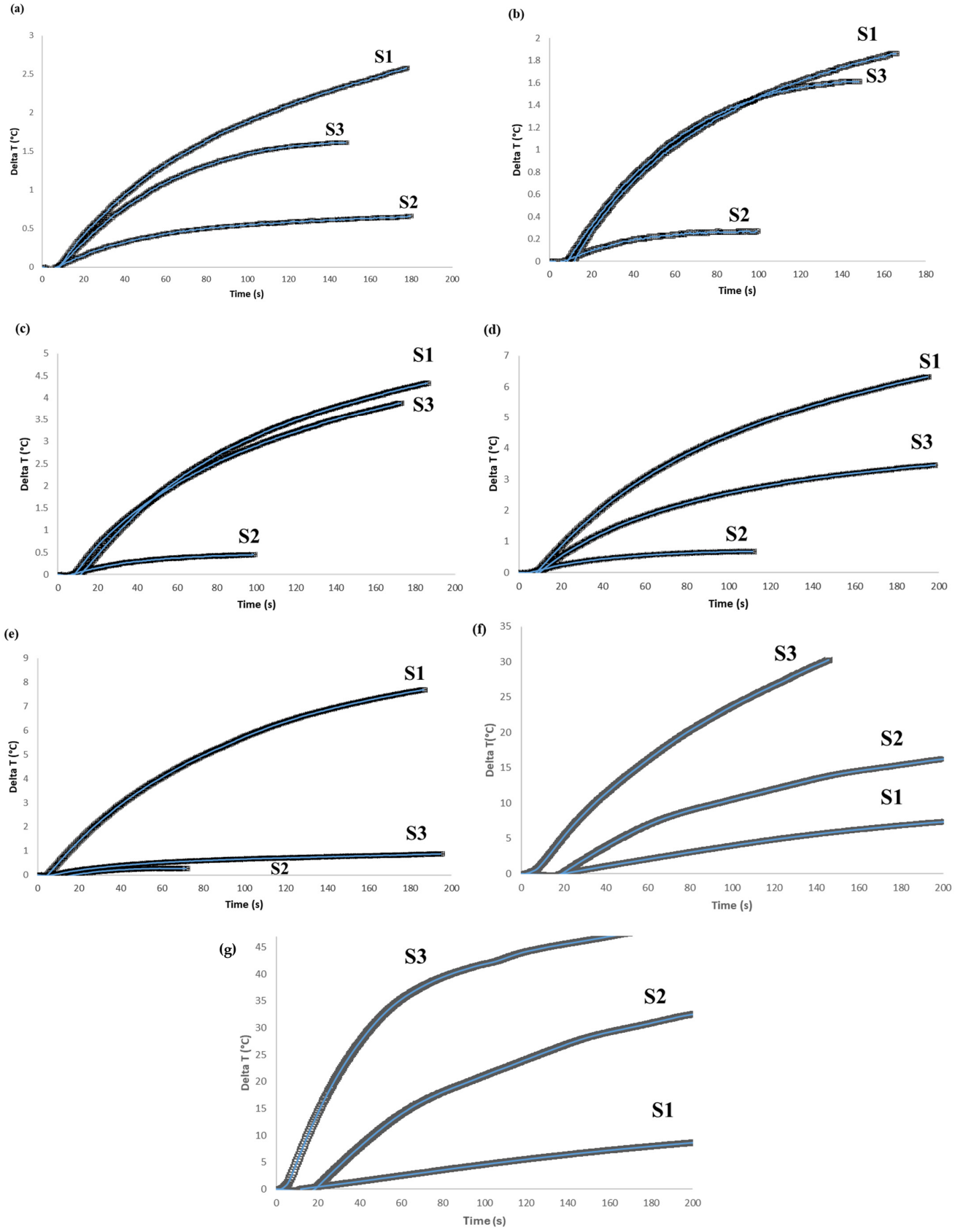


Figure 5. The heating performance of fabricated samples S1, S2, and S3 at (**a**) f = 106.6 kHz, H = 20 kA/m, (**b**) f = 159.8 kHz, H = 13.5 kA/m, (**c**) f = 269.9 kHz, H = 13.5 kA/m, (**d**) f = 381.6 kHz, H = 12.7 kA/m, (**e**) f = 614.4 kHz, H = 9.5 kA/m, (**f**) f = 97 kHz, H = 40 kA/m, and (**g**) f = 97 kHz, H = 50 kA/m.

The heating performances were evaluated under the conditions of low H and high f (Figure 5a,d,e). Under H = 20 kA/m, the highest heating performance (2.5 °C) was detected for sample S1. Under H = 12.7 kA/m, the highest heating performance (6.3 °C) was detected for sample S1, while the lowest heating performance (3.4 °C) was detected for sample S2. Under H = 9.5 kA/m, the highest thermal performance (7.6 °C) was detected for sample S1. The lowest thermal performance (0.84 °C) was detected for sample S2. This is because fields may not be sufficient to saturate the magnetization of the sample S2. In Table 2, the results of this research compared to those gained by conventional coprecipitation techniques are presented [29–37].

Table 2. Compared the results of this research and conventional coprecipitation techniques.

Nanoparticles Type	Size (nm)	Ms (emu/g)	SLP (W/g)	Ref.
Magnetite	10	3	20	[29]
Magnetite	7.5	10	15.5	[30]
Cobalt ferrite	7	32.3–73.1	11–289	[31]
Cobalt ferrite	16.2	68	90.2	[32]
Cobalt ferrite	9–10	59.56	51.8	[33]
Zinc cobalt ferrite	13	70.23	114.98	[34]
Magnetite	12	41.9	75.35	This study
Magnetite doped with cobalt	8	50.7	11.69	This study
Magnetite doped with cobalt/zinc	25	50.6	110	This study

In a medical context, a particle that aggregates easily can cause fatal embolism. The particles exhibit a wide distribution with varied aggregation behavior, which is a major drawback for clinical use, where uniform and stable dispersion is required. Agglomeration significantly reduces heating efficiency. The lower heating efficiency indicates that the sample is dependent on the applied field and agglomeration, which is probably caused by the low stability of the suspension. For instance, the unexpectedly low heating performance of sample S2 was explicitly blamed on extended nanoparticles agglomeration, which leads to a reduction in power dissipation. Composition modification of particles via insertion of a hydrophilic shell could improve their dispersion and heating impact. Magnetite nanoparticles are oxidized in an atmospheric state. This lack of phase purity means the magnetic properties, and thus the heating efficiency, could degrade over time if the particles are not perfectly stored or coated. We tried to overcome this challenge by coating the sample S3 with surfactants (i.e., sodium citrate) to decrease their aggregation and increase their stability. The aggregation between nanoparticles of coated sample S3 was decreased as shown by TEM (Figure 6). In addition, the Zeta potential of coated sample S3 shows enhanced stability with higher Zeta potential compared to uncoated sample S3. Sodium citrate was used as a coating agent for magnetite doped with cobalt/zinc nanoparticles. It could improve the charge surface particles for colloid stability and biocompatible properties.

For hyperthermia efficiency, the heating performance was evaluated at varied field strengths. The heating performance of magnetite doped with cobalt/zinc nanoparticles was optimized with a field strength of 50 kA/m. SLP value was calculated by employing the influence of the coating agent and dispersing solvent to evaluate and optimize the hyperthermia performance.

The impact of the coating agent on SLP was detected; it reduced SLP slightly to 104 W/g (with coating agent) from 110 W/g (without coating agent). The shape modulation and size of particles could result in tuned magnetic properties and further shift the heating performance. The surface-coated layer on the particles protects the core from oxidation, thereby enhancing compatibility and stability for biomedical applications.

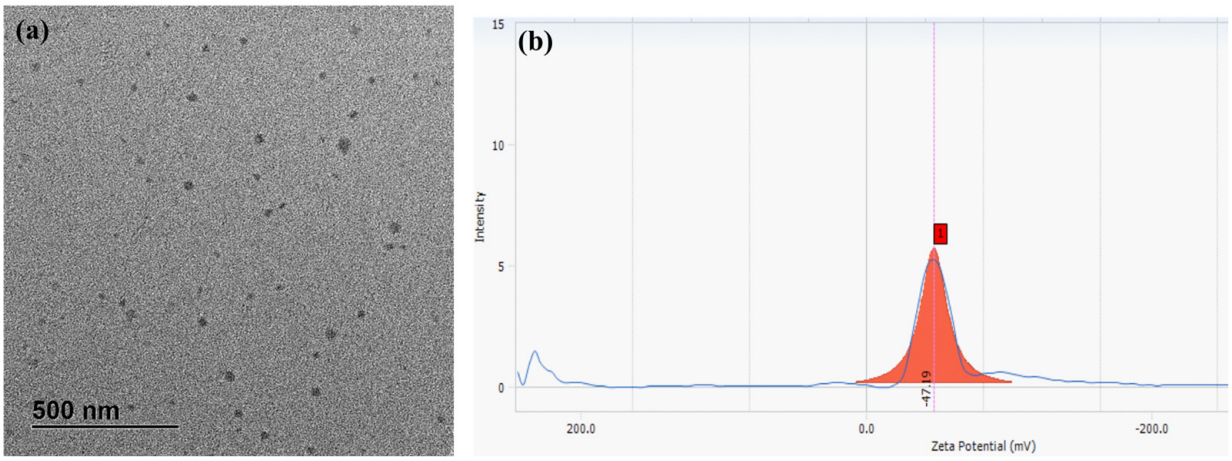


Figure 6. (**a**) TEM, and (**b**) Zeta potential of the fabricated coated sample S3 with sodium citrate.

To evaluate Néel/Brownian contributions to thermal generation, magnetite doped with cobalt/zinc nanoparticles was mixed with glycerol as a high-viscosity solvent. The heating performance decreased with increasing exposure time (Figure 7). The solvent viscosity had a dramatic impact on SLP, reducing it from 110 W/g (water as a solvent) to 7 W/g (glycerol as a solvent). This confirmed that glycerol restricts heat transfer under AMF. Brownian relaxation is restricted by the particles' viscosity, which minimizes the rotation of the particles in the solvent. The medium viscosity impacts the heating performance with a Brownian mechanism, and SLP was reduced.

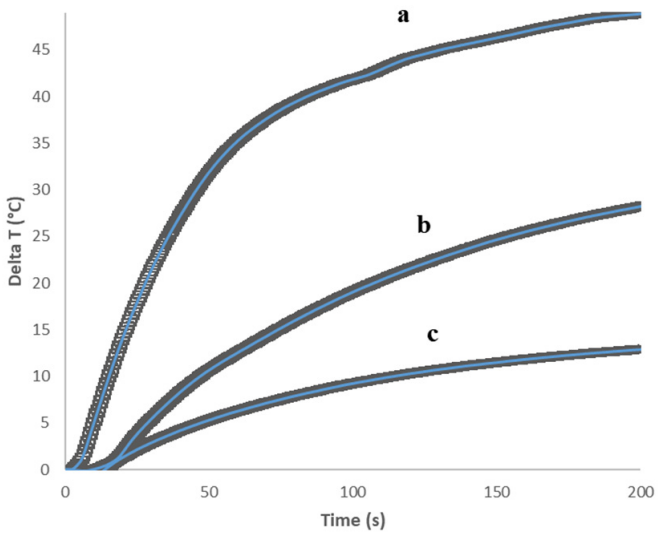


Figure 7. The heating performance at H = 50 kA/m for sample S3 (a) without coating agent, (b) with coating agent, (c) with glycerol.

The cytotoxicity of uncoated sample S3 and coated sample S3 with sodium citrate was studied using in vitro culture with NIH-3T3 fibroblasts (Figure 8). The cell viability for the coated sample S3 particle remained comparatively high, up to 0.5 mg/mL to the control sample, showing that the fabricated particles have a low toxicity. Decrease in cell viability for uncoated sample S3 may be associated with agglomeration, which is probably caused by the low stability of the suspension. Cobalt and zinc can be toxic when they leach from the magnetic core. Citrate coating could improve biocompatibility, where this coating could prevent metal ions leaching in a biological environment.

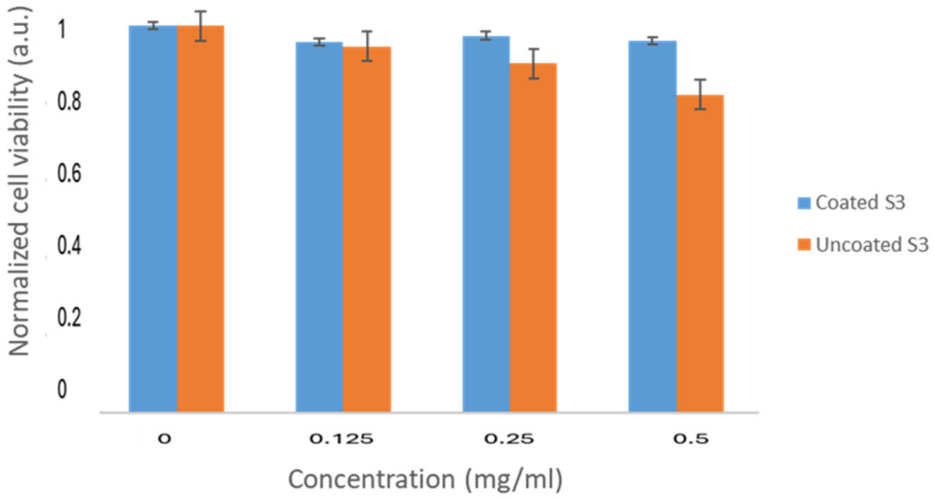


Figure 8. The cytocompatibility tested using a WST assay for the uncoated sample S3 and coated sample S3 with sodium citrate.

4. Discussion

Size and morphology importantly affect a nanoparticle's surface area, reactivity, and magnetic behavior, all of which are critical for its function. The fabricated nanoparticles have a wide distribution with varied aggregation behavior. The standard deviations of the particle size come from measuring many individual particles within one single batch. This only shows that the particles in that specific batch have a distribution of sizes. This is a measure of polydispersity, not experimental reproducibility. Sample S2 showed the smallest size, while inserting zinc in the matrix led to size increase and aggregation. Aggregations are due to dipole/dipole interaction and high surface energy [19]. DLS displays statistical values about hydrodynamic size. Samples show a wider distribution of sizes. DLS analysis performance depends on various parameters such as the particle size, sample shape, concentration, pH, polydispersity, and surface behavior. Scattering may not be enough to have proper detection for a diluted sample. Otherwise, multiple scattering can occur for a concentrated sample.

Sample S3 showed the lowest stability with small electrostatic repulsive force. In contrast, sample S1 exhibited the highest Zeta potential value, which indicates that the particles may show high stability [20–22]. The measurement of ferrites exhibits a positive Zeta potential, where it could protonate (H^+) at low pH. In addition, doping with positive ions (incorporating transition metal, e.g., Fe^{3+}, Co^{2+}, Zn^{2+}) during fabrication can further enhance the positive surface charge. Zeta potential near ±30 mV is confirmed to be associated with stability (presence of high repulsive forces between the particles). Stability is important to obtain expected and regular results [23–25].

The detected peaks at (440), (511), (422), (400), (311), and (220) were approved for the dominant ferrite. However, the presence peaks at (104) (024), (116), and (113) confirmed maghemite (Figure 2) [21,35]. Magnetite nanoparticles could be oxidized in an atmospheric state. A decrease in peak position towards lower 2θ with a decrease in peak intensity was because of the insertion of zinc. The indexed peaks were wide because of small crystallites. The peak extent is affected by strain impact and crystallites.

The ferrite nanoparticles showed high absorption in the visible/near-IR scale, which may be for d-orbital transition. The peak around 400 nm belongs to ferric ions in a tetrahedral coordination [21].

Sample S2 showed the highest magnetization saturation (Ms), which with field increase exerts no improved impact on magnetization and reached saturation. A superparamagnetic condition was reported for cobalt ferrite with size 4.8 nm and Ms 48.8 emu/g [22]. The

magnetization (Ms) is enhanced with the nanoparticle size increased to a maximum, near the bulk magnetization value. Sample S1 showed the lowest coercivity (Hc) as soft magnetic particles, which is the reverse field value wanted to minimize the magnetization from remanence to zero under the reversing field. Samples S2 and S3 showed high coercivity (Hc), where cobalt ions have a primary impact in demonstrating hard magnetic behavior. Sample S1 showed the lowest residual magnetism (Mr), which is the value of magnetization left in a ferromagnetic particle after the field is gone. ZFC/FC (Zero-Field Cooled/Field Cooled) curves are not available. Without ZFC/FC, the blocking temperature cannot be definitively stated, which is essential to prove that the particles will not clump inside a human body at 37 °C.

In this work, the heating performances were investigated by using varied magnetic field conditions to optimize the heating impacts (Figure 5). With time, the temperature was elevated in a linear fashion and then slowed down to a saturation region (Figure 5). In a shorter time, the ferrites nanoparticles became heated rapidly, and by increasing frequency the thermal efficiency increased. Ferrites have high thermal impact with a minimum dose for rapid therapy. When comparing the thermal performance of the fabricated samples, sample S3 showed the highest performance. The magnetic coupling between hard and soft phases may enhance magnetic behavior and anisotropy and possibly result in the improvement of heat-generation efficiency for sample S3. For active hyperthermia therapy, the temperature should reach 6–8 °C to gain (43–45 °C). Hyperthermia techniques require a high magnetic field with high frequency, which is much more challenging for clinical application. This situation requires the development of a material with high efficiency for innovative therapy strategies that minimize side effects and increase treatment effectiveness with minimal technical requirements for clinical applications.

This study's limitation is statistical repeats. The error bars for heating data in the manuscript currently represent measurement variance within a single sample (internal statistics) but do not reflect experimental reproducibility (repeats). This does not account for human error, sample-preparation variability, or environmental factors. It is a theoretical limit, not an experimental measurement.

It is pivotal to maintain H and its f under the safety limit. The safety limit is equal to $H \times f$ and should be $C \leq 5 \times 10^9$ A/ms to reduce side impacts [24–36]. In our research, C was 3.8–4.8 $\times$ 10^9 A/ms for H = 40–50 kA/m. At H = 13.5 kA/m, with f = 159.8–269.9 kHz, C was 2.1–3.6 $\times$ 10^9 A/ms. These rates did not surpass the safety border. However, with H = 9.5 kA/m, the value of C was 5.8 $\times$ 10^9 A/ms, which slightly surpasses the safety border. In this work, sample S3 showed the highest ILP 0.45 nHm2/kg with f = 97 kHz and H = 50 kA/m, regarding safety consciousness on the Atkinson–Brezovich limit ($H \times f$). It was reported that magnetite nanoparticles coated with chitosan showed rapid tumor inhibition via magnetic hyperthermia treatment with ILP = 9.0 [36]. In another report magnetite nanoparticles/PEG exhibited high magnetic hyperthermia performance with ILP = 1.22 [37]. Fuentes-García et al. prepared magnetite nanoparticles via sonochemical technique with good heating performance (ILP = 0.72) [38]. SLP has been utilized to measure absorbed energy per mass of nanoparticles under AMF. In this study, sample S3 demonstrated the highest SLP 110 W/g with f = 97 kHz and H = 50 kA/m, where AMF conditions did not surpass the safety border. Sample S1 detected SLP 75.35 W/g at f = 614.4 kHz and H = 9.5 kA/m. Sample S3 exhibited SLP 44.09 W/g with f = 269.9 kHz, while sample S2 showed the lowest SLP 11.69 W/g with f = 159.8 kHz. The detected decrease in SLP was because of an extended nanoparticle agglomeration under AMF, resulting in a power dissipation reduction and minimized heating efficiency. Great efforts have been made by researchers to gain the smallest nanoparticles possible and to enhance SLP. Bauer et al. fabricated Zn-doped Fe_3O_4 with SLP 1019.2 W/g with H = 16 kA/m

and f = 380 kHz; however, that condition surpassed the safety limit 5 × 10^9 A/ms [25]. Dadfar et al. fabricated citrate-shelled superparamagnetic particles with SLP 350 W/g at H = 46 kA/m and f = 186 kHz [27]. SLP (150 W/g) was obtained with H = 20 mT and f = 205 kHz [28]. Coated Fe_3O_4 exhibited higher SLP (119 W/g) than the uncoated one [29].

5. Conclusions

Magnetic ferrite nanoparticles were fabricated with ultrasonic-assisted coprecipitation techniques to attain nanoparticles with high hyperthermia performance. Magnetite doped with cobalt/zinc nanoparticles exhibited the highest SLP 110 W/g under AMF conditions and did not surpass the safety border. Magnetite doped with cobalt nanoparticles showed the lowest heating performance. The heating performance of magnetite doped with cobalt/zinc nanoparticles increased as the strength increased, while the self-heating performance of magnetite nanoparticles increased as the frequency increased. As a result, the heating performance of magnetite doped with cobalt/zinc shows promise in the field of hyperthermia.

Author Contributions: Conceptualization, methodology, resources, writing—review and editing. E.A.A.-H.; conceptualization, methodology, resources, writing—review and editing, G.H.M.; Conceptualization, methodology, resources, writing—review and editing. J.M.A.-A.; Conceptualization, methodology, writing—original draft, M.S.A.D. All authors have read and agreed to the published version of the manuscript.

Funding: This research received no external funding.

Data Availability Statement: Data are contained within the article.

Conflicts of Interest: The authors declare no conflicts of interest.

References

1. Comanescu, C. Magnetic Nanoparticles: Current Advances in Nanomedicine, Drug Delivery and MRI. *Chemistry* **2022**, *4*, 872–930. [CrossRef]
2. Alamier, W.M.; El-Telbani, E.M.; Syed, I.S.; Bakry, A.M. Cobalt Ferrite Nanoparticles: Highly Efficient Catalysts for the Biginelli Reaction. *Ceramics* **2025**, *8*, 102. [CrossRef]
3. Iacovita, C.; Lucaciu, C.M.; Freis, B.; Kiefer, C.; Bégin-Colin, S. Comparative Influence of Dendron and Dicarboxylate Coatings on the Hyperthermia Performances of Cubic and Spherical Magnetic Nanoparticles. *Int. J. Mol. Sci.* **2025**, *26*, 9324. [CrossRef]
4. Musiał, J.; Jędrzak, A.; Bielas, R.; Skumiel, A. Magnetothermal Energy Conversion of Polydopamine-Coated Iron Oxide Ferrogels Under High-Frequency Rotating Magnetic Fields. *Energies* **2025**, *18*, 4291. [CrossRef]
5. Costa, B.; Carvalho, J.; Gavinho, S.; Vieira, T.; Silva, J.C.; Soares, P.I.P.; Valente, M.A.; Soreto, S.; Graça, M. Preparation and Characterization of Zinc Ferrite and Gadolinium Iron Garnet Composite for Biomagnetic Applications. *Materials* **2024**, *17*, 2949. [CrossRef]
6. Nguyen, M.D.; Hoijang, S.; Yarinia, R.; Ariza Gonzalez, M.; Mandal, S.; Tran, Q.M.; Chinwangso, P.; Lee, T.R. Magnetic Iron Oxide Nanoparticles: Advances in Synthesis, Mechanistic Understanding, and Magnetic Property Optimization for Improved Biomedical Performance. *Nanomaterials* **2025**, *15*, 1500. [CrossRef]
7. Ardeleanu, H.; Ababei, G.; Grigoras, M.; Ursu, L.; Melniciuc-Puica, N.; Astefanoaei, I.; Pricop, D.; Lupu, N.; Creanga, D. Cobalt Ferrite Nanoparticles Capped with Perchloric Acid for Life-Science Application. *Crystals* **2023**, *13*, 1058. [CrossRef]
8. Costa, B.; Pereira, E.; Ferreira-Filho, V.C.; Pires, A.S.; Pereira, L.C.J.; Soares, P.I.P.; Botelho, M.F.; Mendes, F.; Graça, M.P.F.; Teixeira, S.S. Influence of the pH Synthesis of Fe_3O_4 Magnetic Nanoparticles on Their Applicability for Magnetic Hyperthermia: An In Vitro Analysis. *Pharmaceutics* **2025**, *17*, 844. [CrossRef]
9. Sánchez-Cabezas, S.; Montes-Robles, R.; Gallo, J.; Sancenón, F.; Martínez-Máñez, R. Combining magnetic hyperthermia and dual T1/T2 MR imaging using highly versatile iron oxide nanoparticles. *Dalton Trans.* **2019**, *48*, 3883–3892. [CrossRef] [PubMed]
10. Carvalho, A.; Gallo, J.; Pereira, D.; Valentão, P.; Andrade, P.; Hilliou, L.; Ferreira, P.; Bañobre-López, M.; Martins, J. Magnetic Dehydrodipeptide-Based Self-Assembled Hydrogels for Theragnostic Applications. *Nanomaterials* **2019**, *9*, 541. [CrossRef]
11. Le, T.; Phu Bui, M.; Yoon, J. Theoretical Analysis for Wireless Magnetothermal Deep Brain Stimulation Using Commercial Nanoparticles. *Int. J. Mol. Sci.* **2019**, *20*, 2873. [CrossRef]

12. Appa Rao, P.; Srinivasa Rao, K.; Pydi Raju, T.R.K.; Kapusetti, G.; Choppadandi, M.; Chaitanya Varma, M.; Rao, K.H. A systematic study of cobalt-zinc ferrite nanoparticles for self-regulated magnetic hyperthermia. *J. Alloys Compd.* **2019**, *794*, 60–67. [CrossRef]
13. Apostolov, A.; Apostolova, I.; Wesselinowa, J. Specific absorption rate in Zn-doted ferrites for self-controlled magnetic hyperthermia. *Eur. Phys. J. B* **2019**, *92*, 3. [CrossRef]
14. Mai, B.T.; Balakrishnan, P.B.; Barthel, M.J.; Piccardi, F.; Niculaes, D.; Marinaro, F.; Fernandes, S.; Curcio, A.; Kakwere, H.; Autret, G.; et al. Thermoresponsive Iron Oxide Nanocubes for an Effective Clinical Translation of Magnetic Hyperthermia and Heat-Mediated Chemotherapy. *ACS Appl. Mater. Interfaces* **2019**, *11*, 5727–5739. [CrossRef] [PubMed]
15. Gupta, R.; Sharma, D. Evolution of Magnetic Hyperthermia for Glioblastoma Multiforme Therapy. *ACS Chem. Neurosci.* **2019**, *10*, 1157–1172. [CrossRef]
16. Makridis, A.; Curto, S.; van Rhoon, G.C.; Samaras, T.; Angelakeris, M. A standardisation protocol for accurate evaluation of specific loss power in magnetic hyperthermia. *J. Phys. D Appl. Phys.* **2019**, *52*, 255001. [CrossRef]
17. Shaw, S.K.; Biswas, A.; Gangwar, A.; Maiti, P.; Prajapat, C.L.; Singh Meena, S.; Prasad, N.K. Synthesis of exchange coupled nanoflowers for efficient magnetic hyperthermia. *J. Magn. Magn. Mater.* **2019**, *484*, 437–444. [CrossRef]
18. Dadfar, S.; Camozzi, D.; Darguzyte, M.; Roemhild, K.; Varvara, P.; Metselaar, J.; Banala, S.; Straub, M.; Guvener, N.; Engelmann, U.; et al. Size-isolation of superparamagnetic iron oxide nanoparticles improves MRI, MPI and hyperthermia performance. *J. Nanobiotechnol.* **2020**, *18*, 22. [CrossRef] [PubMed]
19. Ayyappan, S.; Mahadevan, S.; Chandramohan, P.; Srinivasan, M.P.; Philip, J.; Raj, B. Influence of Co^{2+} Ion Concentration on the Size, Magnetic Properties, and Purity of $CoFe_2O_4$ Spinel Ferrite Nanoparticles. *J. Phys. Chem. C* **2010**, *114*, 6334–6341. [CrossRef]
20. Darwish, M.S.A.; Stibor, I. Pentenoic Acid-Stabilized Magnetic Nanoparticles for Nanomedicine Applications. *J. Dispers. Sci. Technol.* **2016**, *37*, 1793–1798. [CrossRef]
21. Badawy, S.M.; Abd, E.-L. Synthesis and characterizations of magnetite nanocomposite films for radiation shielding. *Polym. Compos.* **2017**, *38*, 974–980. [CrossRef]
22. Pereira, C.; Pereira, A.M.; Fernandes, C.; Rocha, M.; Mendes, R.; Fernández-García, M.P.; Guedes, A.; Tavares, P.B.; Grenèche, J.M.; Araújo, J.P.; et al. Superparamagnetic MFe_2O_4 (M = Fe, Co, Mn) Nanoparticles: Tuning the Particle Size and Magnetic Properties through a Novel One-Step Coprecipitation Route. *Chem. Mater.* **2012**, *24*, 1496–1504. [CrossRef]
23. Darwish, M.S.A. Effect of carriers on heating efficiency of oleic acid-stabilized magnetite nanoparticles. *J. Mol. Liq.* **2017**, *231*, 80–85. [CrossRef]
24. Hergt, R.; Dutz, S. Magnetic particle hyperthermia—Biophysical limitations of a visionary tumour therapy. *J. Magn. Magn. Mater.* **2007**, *311*, 187–192. [CrossRef]
25. Bauer, L.; Situ, S.; Griswold, M.; Samia, A. High-performance iron oxide nanoparticles for magnetic particle imaging-guided hyperthermia (hMPI). *Nanoscale* **2016**, *8*, 12162–12169. [CrossRef] [PubMed]
26. Hergt, R.; Dutz, S.; Muller, R.; Zeisberger, M. Magnetic particle hyperthermia: Nanoparticle magnetism and materials development for cancer therapy. *J. Phys. Condens. Matter* **2006**, *18*, S2919. [CrossRef]
27. Nigam, S.; Barick, K.; Bahadur, D. Development of citrate-stabilized Fe3O4 nanoparticles: Conjugation and release of doxorubicin for therapeutic applications. *J. Magn. Magn. Mater.* **2011**, *323*, 237–243. [CrossRef]
28. Shete, P.B.; Patil, R.M.; Thorat, N.D.; Prasad, A.; Ningthoujam, R.S.; Ghosh, S.J.; Pawar, S.H. Magnetic chitosan nanocomposite for hyperthermia therapy application: Preparation, characterization and in vitro experiments. *Appl. Surf. Sci.* **2014**, *288*, 149. [CrossRef]
29. Le Renard, P.; Lortz, R.; Senatore, C.; Rapin, J.; Buchegger, F.; Petri-Fink, A.; Hofmann, H.; Doelker, E.; Jordan, O. Magnetic and in vitro heating properties of implants formed in situ from injectable formulations and containing superparamagnetic iron oxide nanoparticles (SPIONs) embedded in silica microparticles for magnetically induced local hyperthermia. *J. Magn. Magn. Mater.* **2011**, *323*, 1054–1063. [CrossRef]
30. Ma, M.; Wu, Y.; Zhou, J.; Sun, Y.; Zhang, Y.; Gu, N. Size dependence of specific power absorption of Fe_3O_4 particles in AC magnetic field. *J. Magn. Magn. Mater.* **2004**, *268*, 33–39. [CrossRef]
31. Manjura Hoquea, S.; Huanga, Y.; Coccod, E.; Maritimc, S.; Santind, A.D.; Shapiroe, E.M.; Comana, D.; Hyder, F. Improved specific loss power on cancer cells by hyperthermia and MRI contrast of hydrophilic $Fe_xCo_{1-x}Fe_2O_4$ nanoensembles. *Contrast Media Mol. Imaging* **2016**, *11*, 514–526. [CrossRef] [PubMed]
32. Durneata, D.; Hempelmann, R.; Caltun, O.; Dumitru, I. High-Frequency Specific Absorption Rate of $Co_xFe_{1-x}Fe_2O_4$ Ferrite Nanoparticles for Hipertermia Applications. *IEEE Trans. Magn.* **2014**, *50*, 5201104. [CrossRef]
33. Pradhan, P.; Giri, J.; Samanta, G.; Sarma, H.D.; Mishra, K.P.; Bellare, J.; Banerjee, R.; Bahadur, D. Comparative evaluation of heating ability and biocompatibility of different ferrite-based magnetic fluids for hyperthermia application. *J. Biomed. Mater. Res. Part B Appl. Biomater.* **2007**, *81*, 12–22. [CrossRef] [PubMed]
34. Nikam, D.S.; Jadhav, S.V.; Khot, V.M.; Phadatare, M.R.; Pawar, S.H. Study of AC magnetic heating characteristics of $Co_{0.5}Zn_{0.5}Fe_2O_4$ nanoparticles for magnetic hyperthermia therapy. *J. Magn. Magn. Mater.* **2014**, *349*, 208–213. [CrossRef]

35. Song, H.K.; Sonkaria, S.; Khare, V.; Dong, K.; Lee, H.-T.; Ahn, S.-H.; Kim, H.-K.; Kang, H.-J.; Lee, S.-H.; Jung, S.P.; et al. Pond Sediment Magnetite Grains Show a Distinctive Microbial Community. *Microb. Ecol.* **2015**, *70*, 168–174. [CrossRef]
36. Chauhan, A.; Midha, S.; Kumar, R.; Meena, R.; Singh, P.; Jhab, S.; Kuanr, K. Rapid tumor inhibition via magnetic hyperthermia regulated by caspase 3 with time-dependent clearance of iron oxide nanoparticles. *Biomater. Sci.* **2021**, *9*, 2972–2990. [CrossRef]
37. Liu, X.L.; Fan, H.M.; Yi, J.B.; Yang, Y.; Choo, E.S.G.; Xue, J.M.; Ding, J. Optimization of surface coating on Fe3O4 nanoparticles for high performance magnetic hyperthermia agents. *J. Mater. Chem.* **2012**, *22*, 8235–8244. [CrossRef]
38. Fuentes-García, J.A.; Carvalho Alavarse, A.; Moreno Maldonado, A.C.; Toro-Córdova, A.; Ibarra, M.R.; Goya, G.F. Simple Sonochemical Method to Optimize the Heating Efficiency of Magnetic Nanoparticles for Magnetic Fluid Hyperthermia. *ACS Omega* **2020**, *5*, 26357–26364. [CrossRef]

Disclaimer/Publisher's Note: The statements, opinions and data contained in all publications are solely those of the individual author(s) and contributor(s) and not of MDPI and/or the editor(s). MDPI and/or the editor(s) disclaim responsibility for any injury to people or property resulting from any ideas, methods, instructions or products referred to in the content.